

Poly(3,4-ethylenedioxythiophene)–Multiwalled Carbon Nanotube Composite Films: Structure-Directed Amplified Electrochromic Response and Improved Redox Activity

Shweta Bhandari,[†] Melepurath Deepa,^{*,†} Avanish Kumar Srivastava,[†] Amish G. Joshi,[†] and Rama Kant[‡]

National Physical Laboratory, Dr. K.S. Krishnan Road, New Delhi 110012, India, and Department of Chemistry, University of Delhi, New Delhi 110007, India

Received: February 12, 2009; Revised Manuscript Received: May 21, 2009

Composite thin films of poly(3,4-ethylenedioxythiophene) (PEDOT)-enwrapped functionalized multiwalled carbon nanotubes (MWCNTs) have been synthesized over multiple length scales by electropolymerization of the monomer without the use of any other supporting electrolyte. The functionalized MWCNTs are incorporated into the positively charged polymer deposit as counterions during oxidative electropolymerization. The morphology, electrochemistry, and electrochromism of the PEDOT–MWCNT films have been compared with those of control PEDOT films doped by triflate ions. Such a comparison enabled us to demonstrate the profound effect of MWCNTs as counterions, realized in terms of better electropolymerization rate, higher conductivity, faster color–bleach kinetics, higher charge storage capacity, and substantially amplified coloration efficiency ($\eta = 414 \text{ cm}^2 \text{ C}^{-1}$, $\lambda_{\max} = 575 \text{ nm}$, $E = -1.5 \text{ V}$) in comparison to the values of η reported to date for PEDOT. The strong interaction between the polymer and MWCNTs, the interconnected nanotubular structures, and the porous framework of the film allow facile charge transport and larger ion uptake during redox switching. Electrochemical investigations on devices based on PEDOT–MWCNT and control PEDOT films established the practical utility of PEDOT–MWCNT films as they show lower charge-transfer resistance, higher diffusional capacitance, and a much smaller amplitude of impedance as compared to control PEDOT films.

1. Introduction

The addition of carbon nanotubes (CNTs) to the carbon family way back in the 1990s¹ has provided a fertile area of innovative material science and nanotechnology opportunities because of their unparalleled mechanical and electronic properties.^{2–4} Recent research has sought to integrate carbon nanotubes into more complex assemblies like polymers,^{5,6} driven by their synergic contributory effects.⁷ CNT/polymer nanocomposites have evoked enormous interest as a new class of advanced materials for their broad range of applications ranging from general low-cost circuits to high-power supercapacitors,^{8,9} sensors,¹⁰ and displays.¹¹ Depending on the application, the polymers could be either insulating^{12,13} or conducting.^{14,15}

The high aspect ratio of CNTs resulting from the arrangement of strong carbon–carbon covalent bonds oriented along the *c*-axis of nanotubes provides a great mechanical strength to the composite material. CNTs are therefore like mechanical springs, which are one of the stiffest structures ever made, and at the same time, these can be flattened or buckled to accommodate larger loads.¹⁶ Besides providing mechanical strength to the polymer matrix, the network-like structure of the CNT provides channels for electrical percolation that considerably improves the conductivity and other electrochemical properties of the composites.¹⁷ Their low dissipation energy enables them to carry tremendous current densities as well.¹⁸ However, the exploitation of their properties in composites is itself a challenge due to the agglomerating tendency and poor dispersibility of pristine CNTs

in common solvents caused by the strong intertube van der Waals interactions.⁷ Several successful attempts have been made earlier by adsorption of surfactants¹⁹ and polymers²⁰ in the walls of CNTs during sonication, but complete removal of surfactant molecules is not easy. On the other hand, the drawback of excessive chemical modification is that it adversely affects the functional properties of CNTs. To circumvent this problem, mild oxidation via acid treatment utilizing the pentagonal defects residing on the ends of nanotubes provides an adroit route with fewer adversities, making them more amenable to rational manipulation.²¹ The carboxyl and hydroxyl functionalities generated by acid treatment impart negative charge to the CNTs, which not only stabilizes the ensuing dispersion in an aqueous medium but also helps CNTs to function as dopants during the electropolymerization process when mixed with monomers. To date, the understanding of structure and electroactivity of conducting polymer–CNTs is rather limited as very few reports have addressed this issue.^{22,23}

Earlier, electrochemical co-deposition of CNTs with poly-pyrrole²⁴ and polyaniline²⁵ has been reported, resulting in more conductive and capacitive polymer composite films. Few authors have also worked on the electrochemical and optical monitoring of PEDOT by multiwalled carbon nanotubes (MWCNTs),²⁶ but the effect of the resulting morphology on the electrochromic aspects has not been surmised upon. Further, reports wherein the electrochemistry of solid-state electrochromic devices based on PEDOT–MWCNT films has been evaluated are almost nonexistent. In the present report, an aqueous dispersion of functionalized MWCNTs and 3,4-ethylenedioxythiophene (EDOT) was made, and electropolymerization yielded composites of MWCNT-doped polymer deposits. Doping PEDOT with nega-

* To whom correspondence should be addressed. Tel: +91-11-45608283. E-mail: m_deepa@mail.nplindia.ernet.in.

[†] National Physical Laboratory.

[‡] University of Delhi.

tively charged MWCNTs imparts the films with both enhanced electronic and ionic conductivity, along with better electro-optical and redox properties. In the work presented here, the significant impact of the functionalized MWCNTs as dopants attached to the polymer backbone realized in terms of much improved electrochemical activity, coloration efficiency, and switching kinetics as compared to control PEDOT films grown in a conventional electrolyte has been discussed in detail to prove the applicability of the PEDOT—MWCNT electrodes in electrochromic devices. Composite formation of MWCNTs with PEDOT has been confirmed by X-ray photoelectron spectroscopy (XPS) and high-resolution transmission electron microscopy (HRTEM), and this has been shown to be a material with sufficient leverage in its properties to extend its use as the functional electrode in devices other than electrochromic devices.

2. Experimental Section

2.1. Chemicals. 3,4-Ethylenedioxythiophene or EDOT (Aldrich), was used as received. Lithium perchlorate (LiClO_4) and lithium trifluoromethane sulfonate (LiCF_3SO_3) were purchased from Aldrich and dried under vacuum at 120 °C for 24 h prior to use. Poly(vinyl alcohol) ($M_w \sim 85000$ –146000) was obtained from Aldrich. Inorganic transparent electrodes of SnO_2/F -coated glass (Pilkington, sheet resistance: 14 Ω/sq) were cleaned in a soap solution, 30% HCl solution, double distilled water, acetone, and trichloroethylene (in that order) prior to use. Deionized water (resistivity $\sim 18.2 \text{ M}\Omega \text{ cm}$) obtained through Milli-Q system and ethanol (Merck) and dimethyl sulfoxide (DMSO) (Merck) were used as solvents.

2.2. Multiwalled CNT Synthesis and Functionalization. Multiwalled CNTs were synthesized using toluene as a precursor material in a quartz tube in an argon atmosphere with ferrocene as a source of metal catalyst via a catalytic chemical vapor deposition technique. The resulting MWCNTs with diameters in the range of 20–80 nm and lengths ranging from 50 to 100 μm (yield $\sim 90\%$) were functionalized by oxidation with nitric acid.²⁷ The metal particles were also removed during this treatment. The resulting functionalized MWCNTs (functionalized MWCNTs have been referred to as f-MWCNTs/MWCNTs) were then repeatedly washed with water and ethanol and then dried in an oven at 60 °C for half of an hour.

2.3. Deposition of Films. An aqueous solution of 0.1 M EDOT and 0.1 M LiCF_3SO_3 was prepared in deionized water and ethanol (1:1 by volume) for control PEDOT films. A colloidal dispersion of the functionalized MWCNTs (2 mg/mL) in deionized water added to an equal volume of ethanol and polyethylene glycol 400 (mixed in the ratio of 4:1 by volume) containing 0.1 M EDOT was used for PEDOT—MWCNT films. Both of the solutions were magnetically stirred at room temperature for 20 minutes. The control films of PEDOT and the PEDOT—MWCNT composite films were fabricated from the two electropolymerization baths under similar conditions at room temperature (25 ± 2 °C) in a glass cell with a transparent conducting substrate (SnO_2/F -coated glass) as the working electrode, a Pt sheet as the counter electrode, and a $\text{Ag}/\text{AgCl}/\text{KCl}$ reference electrode under potentiostatic conditions (+1.2 V) for about 8 min. The resulting blue colored films of PEDOT were immediately rinsed with deionized water and ethanol and dried in air for 2 hours and stored in air.

2.4. Characterization Techniques. FTIR spectra for the films were recorded in transmission mode with a Perkin—Elmer (Spectrum BX) spectrophotometer at 28 °C, RH ~ 50 –53%. XPS spectra were recorded for the as-synthesized PEDOT films using a Perkin—Elmer 1257 model operating at a base pressure

of 7.8×10^{-8} Torr at 300 K with a nonmonochromatized Al $\text{K}\alpha$ line at 1486.6 eV, an analyzer pass energy of 60 eV, and a hemispherical sector analyzer capable of 25 meV resolution. The overall instrumental resolution was about 0.3 eV. The core level spectra were deconvoluted using a nonlinear iterative least-squares Gaussian fitting procedure. For all fitting doublets, the FWHMs were fixed accordingly. Corrections due to charging effects were taken care of by using C(1s) as an internal reference and the Fermi edge of a gold sample. The surface morphological features of films were investigated using a scanning electron microscope (SEM, LEO 440). For TEM, thin layers of the samples were carefully extracted using forceps in deionized water and then transferred onto a carbon-coated copper grid of 3.05 mm in diameter, and solvent was evaporated at room temperature before use. Transmission electron microscopy was carried out on a TEM, JEOL JEM 200CX, operated at an electron accelerating voltage of 200 kV and high-magnification lattice scale imaging was carried out by employing a transmission electron microscope HRTEM Tecnai G² F30 STWIN with a FEG source at 300 kV. Atomic force microscopy (AFM) images were taken by using molecular imaging (MI), U.S.A. make AFM equipment, in noncontact mode. Cyclic voltammetry (CV) for the films was performed in a classical three-electrode electrochemical cell on an Omni potentiostat, wherein the PEDOT film deposited on SnO_2/F -coated glass acted as the working electrode, a Ag/Ag^+ was employed as the reference electrode, and a Pt rod was used as the auxiliary electrode in a liquid electrolyte (1 M LiClO_4 —propylene carbonate (PC)). The electronic conductivities of functionalized MWCNTs, PEDOT—MWCNT, and control PEDOT were obtained by transferring the films from the substrates into a circular cavity (0.5 cm in diameter) in the center of a sample holder made of mica and sandwiching the same between two stainless steel electrodes, which in turn were insulated from one another by Teflon rings. I – V characteristics were obtained by linear sweep voltammetry (LSV), wherein the voltage was swept from –3.0 to +3.0 V. Ionic conductivity under different dc potentials was determined by electrochemical impedance spectroscopy (EIS) in a liquid electrolyte. The optical density for coloration efficiency calculations was measured ex situ in a Perkin—Elmer Lambda 25 spectrophotometer in 1 M LiClO_4 —PC. An automated setup comprising a He—Ne laser ($\lambda = 632.8$ nm), a Si photodetector, and a custom-made microprocessor-controlled versatile unit was used to record the switching time characteristics for the films between colored and bleached states. A prototype device with PEDOT—MWCNT and Prussian blue films as the cathode and anode, containing a solid polymer gel electrolyte film of 0.2 M LiCF_3SO_3 —dimethyl sulfoxide and 6 wt % poly(vinyl alcohol), was fabricated, and another equivalent device with control PEDOT film as the cathodic layer was also prepared. All electrochemical measurements for devices and films were performed on a Gamry reference 600 potentiostat/galvanostat/ZRA with PHE 200/EIS 300 software, unless specified otherwise.

3. Results and Discussion

3.1. I – t Plots. The current–time transients for electropolymerization of the two films at a constant potential of +1.2 V for 8 min are shown in Figure 1. At $t = 0$, when the potential is applied, the current rises, and peaks are observed in both PEDOT—MWCNT and control PEDOT films with peak heights of 0.004 and 0.0015 A, respectively, and these arise due to double-layer capacitance charge.²⁸ Thereafter, the current shows an exponential decay corresponding to the nucleation and growth of the polymer. The control film shows a plateau after exponential decay, but in the PEDOT—MWCNT film, the

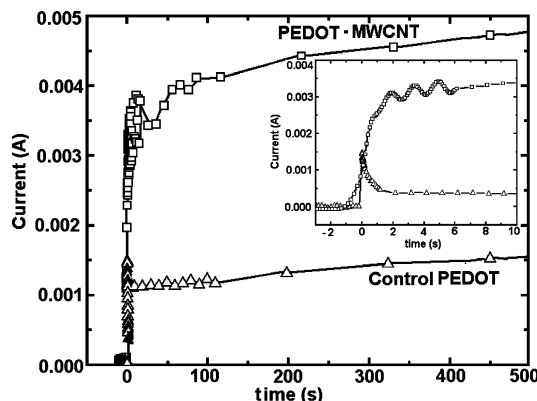


Figure 1. Current–time transients for oxidative electropolymerization of 0.1 M 3,4-(ethylenedioxythiophene) to yield PEDOT–MWCNT (\square) and control PEDOT films (\triangle) in functionalized MWCNTs and lithium trifluoromethanesulfonate based media, respectively. Inset shows the corresponding deposition profiles in the early stages.

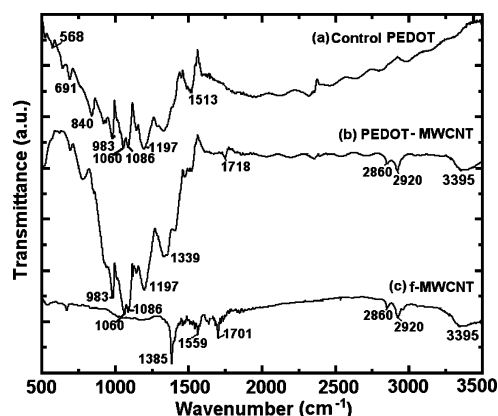


Figure 2. FTIR spectra of (a) control PEDOT, (b) PEDOT–MWCNT films, and (c) functionalized MWCNTs in the 500–3500 cm^{-1} wavenumber region in transmission mode.

current increases again prior to acquisition of the plateau-like response (the inset of Figure 1 shows this feature). The oligomerization process that occurs at the interface just before polymerization is less efficient in the control film, and therefore, there was no further current increase after exponential decay.²⁹ The electropolymerization charge deduced for the PEDOT–MWCNT film is 854 $\mu\text{C cm}^{-2}$, and it is considerably higher than that achieved for the control PEDOT film ($93 \mu\text{C cm}^{-2}$) for the same duration of deposition, thus signifying higher electrodeposition efficiency in the former. The presence of MWCNTs in the precursor solution accelerates the oxidation rate of the monomer, as has been previously established for

polyaniline,³⁰ and the operating principle is stipulated as follows; the oligomeric species and MWCNTs are adsorbed on the substrate, and due to the heterogeneous nature of the initial layer, which also has a higher surface area due to MWCNTs, the polymer chains grow more readily than they do in the control film, thus leading to a core–shell morphology for the ensuing deposit, wherein the MWCNTs are the core and the polymer is the shell. Proof of this is also perceptible from the TEM micrograph (Figure 7a) of the composite PEDOT–MWCNT film.

3.2. FTIR and XPS Studies. The FTIR reflectance spectra of PEDOT, PEDOT–MWCNT, and functionalized MWCNTs (f-MWCNT) are shown in Figure 2. The appearance of $\text{C}=\text{O}$ stretch absorption at 1701 cm^{-1} ³¹ confirms the functionalization of the MWCNTs in Figure 2c, and it blue shifts to 1718 cm^{-1} in the PEDOT–MWCNT film, thus reiterating the inclusion of MWCNT in the polymer film (Figure 2b). Composite formation of PEDOT with MWCNTs is confirmed from the presence of additional peaks seen in the spectrum of the PEDOT–MWCNT film in comparison to the control PEDOT film. The $\nu(\text{C}=\text{O})$ (1701 cm^{-1}) vibrational mode in the PEDOT–MWCNT film is not observed in the control PEDOT film, and the $\nu(-\text{CH}_2-)$ modes are also absent. The $-\text{CH}_2-$ stretching modes at 2860 and 2920 cm^{-1} that appear in the spectrum of functionalized MWCNTs (Figure 2c) are attributable to bonds formed due to sp^3 defects,³² and these modes are retained in the spectrum of the composite PEDOT–MWCNT film (Figure 2b). The spectrum of the control PEDOT film is devoid of these absorptions. The remaining peak assignments have been made according to those tabulated by Garreau et al.,³³ and these are listed in Table 1.

The formation of the PEDOT–MWCNT composite was also ascertained from the comparison of XPS core level spectra of PEDOT–MWCNT and control PEDOT films (Figure 3). The deconvolution of the highly asymmetric C1s photoemission into four components yielded peaks at 284.7, 285.9, 286.7, and 288.2 eV due to the C–C of PEDOT and MWCNTs, the C–S and C–O of PEDOT, and the C=O of the functionalized MWCNT in the composite film (Figure 3a). The complex envelope of C1s of the control PEDOT also contains four peaks at 284.5, 285.5, 286.4, and 287.8 eV, as shown in Figure 3a'; however, the contribution of the highest-energy peak of C=O of PEDOT–MWCNT is replaced by the C–F peak in the control PEDOT film, wherein CF_3SO_3^- was the counterion used for doping PEDOT. The latter is also augmented by the appearance of the F1s signature peak of the control PEDOT film at 687.7 eV (inset of Figure 3a'). The O1s signal ($\text{fwhm} \approx 2.1 \text{ eV}$) is composed of two components in both of the films but involve contributions from different chemical bonds. The peaks at 533.0

TABLE 1: FTIR Peak Assignments for Control PEDOT, PEDOT–MWCNT, and Functionalized MWCNTs

wavenumbers (cm^{-1})	f-MWCNTs	PEDOT–MWCNT	PEDOT
691			symmetric C–S–C deformation
568, 840, 983		oxyethylene ring deformation	oxyethylene ring deformation
1060, 1086		C–O–C deformation	C–O–C deformation
1330		C–C stretch	
1385	non-carbonyl C–O stretching vibrations		asymmetric C=C stretch
1513			
1559	($-\text{CH}_2-$) _n deformation		
1701, 1718	$\text{C}=\text{O}$ stretching of COOH	$\text{C}=\text{O}$ stretching of COOH	
2860, 2920	$\text{C}-\text{H}_2$ stretching indicating the presence of sp^3 defects	$\text{C}-\text{H}_2$ stretching indicating the presence of sp^3 defects	
3395	OH stretching vibrations (hydration)	OH stretching vibrations (hydration)	

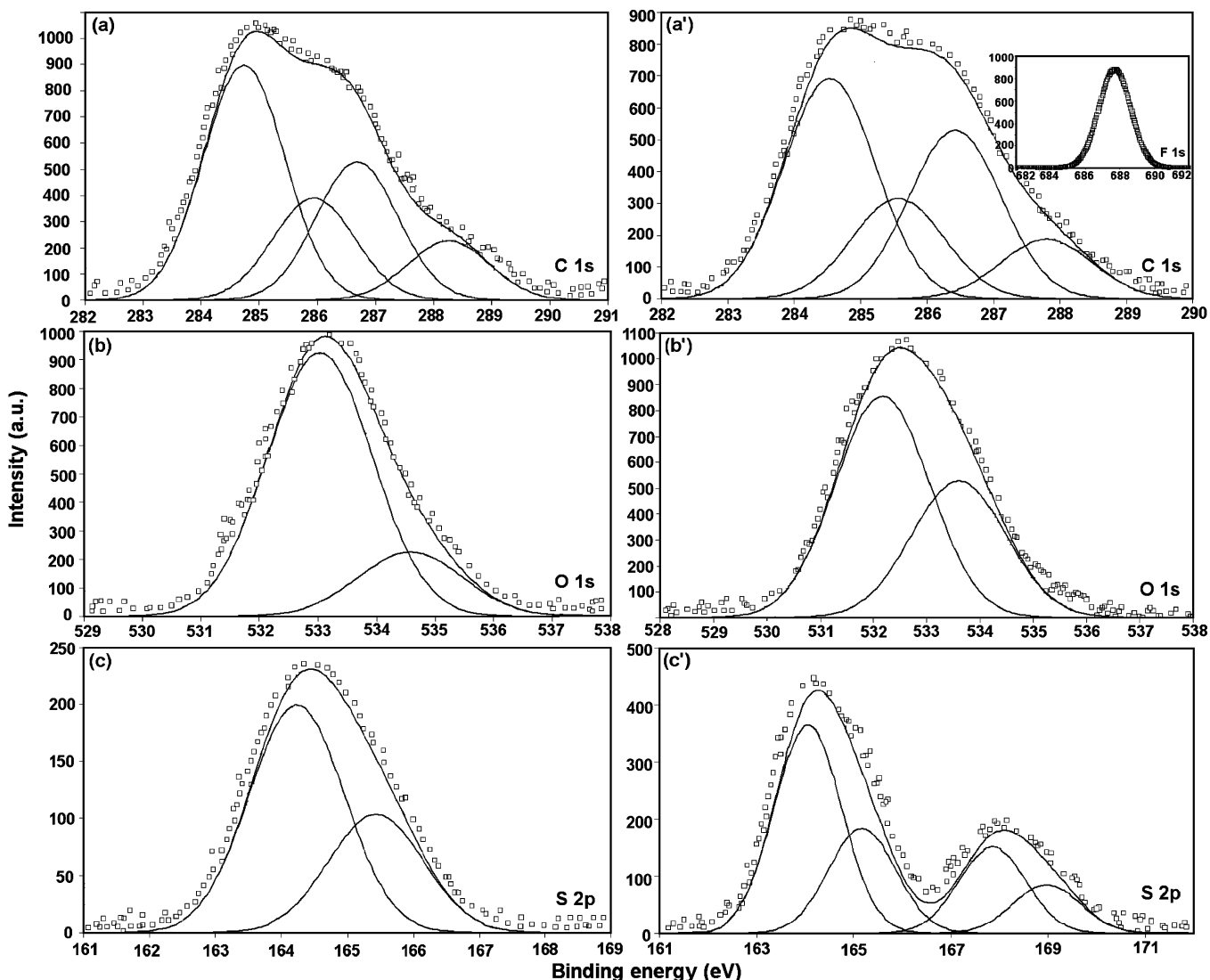


Figure 3. XPS core level spectra of (a, a') C1s, (b, b') O1s, and (c, c') S2p of PEDOT–MWCNT and control PEDOT films, respectively, with solid lines signifying their deconvoluted contributions. The inset of (a') shows the peak of F1s due to the dopant ion.

and 534.6 in the PEDOT–MWCNT film correspond to the O=C of CNTs and the O–C of PEDOT (Figure 3b), whereas in the control PEDOT film (Figure 3b'), the O–C of PEDOT produces a peak at 533.6 eV, and the lower energy peak arises from O=S bonds of the dopant triflate ions. The S2p core level spectrum of PEDOT–MWCNT (Figure 3c) is comprised of a single broad peak with a distinctive shoulder, suggestive of the contributions from the S2p_{3/2} and S2p_{1/2} spin–spin doublet characterized by a fixed 2:1 intensity ratio with an energy splitting of 1.2 eV.^{34,35} In the control PEDOT, the two S2p components arising from the polymer backbone and from the dopant triflate are well resolved (Figure 3c'), the higher binding energy peaks at 167.8 and 168.9 eV being from sulfur in CF_3SO_3^- .

Since O–C=O groups on functionalized MWCNTs are the link-forming moieties with the polymer matrix, the level of doping by functionalized MWCNT in the PEDOT–MWCNT film has been deduced from the $I_{\text{C}=\text{O}(\text{MWCNT})(\text{O}1s)}/I_{\text{C}(\text{PEDOT})(\text{C}1s)}$ and $I_{\text{C}=\text{O}(\text{MWCNT})(\text{O}1s)}/I_{\text{S}(\text{PEDOT})(\text{S}2p)}$ atomic ratios, where $I_{\text{C}=\text{O}(\text{MWCNT})(\text{O}1s)}$ is the percent contribution of oxygen in the C=O of MWCNTs and $I_{\text{C}(\text{PEDOT})(\text{C}1s)}$ and $I_{\text{S}(\text{PEDOT})(\text{S}2p)}$ are of total carbon and total sulfur in PEDOT in the core level spectra of the PEDOT–MWCNT film. These ratios are 0.22 and 0.20, respectively, and as the two values are comparable, this seems to be a reasonable

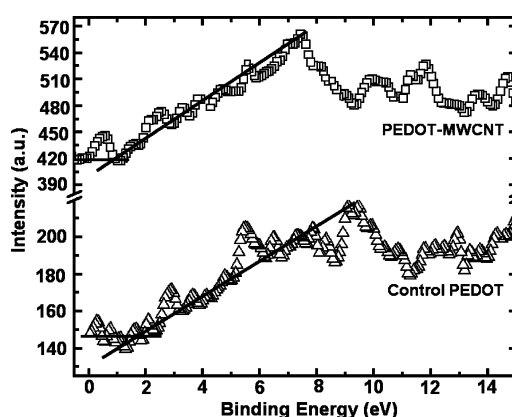


Figure 4. Valence band spectra of PEDOT–MWCNT (□) and control PEDOT films (△) displaying their respective Fermi edges.

estimate of functionalized MWCNTs incorporated into the PEDOT–MWCNT composite film. The dopant level in the control sample is determined from the $I_{\text{S}=\text{O}(\text{CF}_3\text{SO}_3)(\text{S}2p)}/I_{\text{C}(\text{PEDOT})(\text{C}1s)}$ atomic ratio, which is 0.34. Here, $I_{\text{S}=\text{O}(\text{CF}_3\text{SO}_3)(\text{S}2p)}$ is the percent contribution of sulfur in CF_3SO_3^- , and $I_{\text{C}(\text{PEDOT})(\text{C}1s)}$ is that of the total carbon of PEDOT. It is evident that the dopant level of the PEDOT–MWCNT film is lower than that of the control

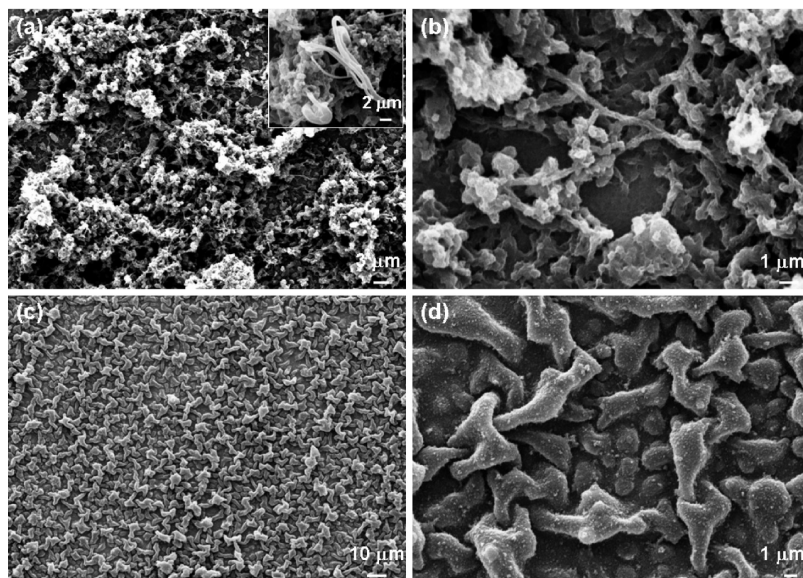


Figure 5. SEM images of (a, b) PEDOT–MWCNT showing bundles of polymer nanofibers enwrapping MWCNTs and (c, d) control PEDOT consisting of closely packed particles, several micrometers in size.

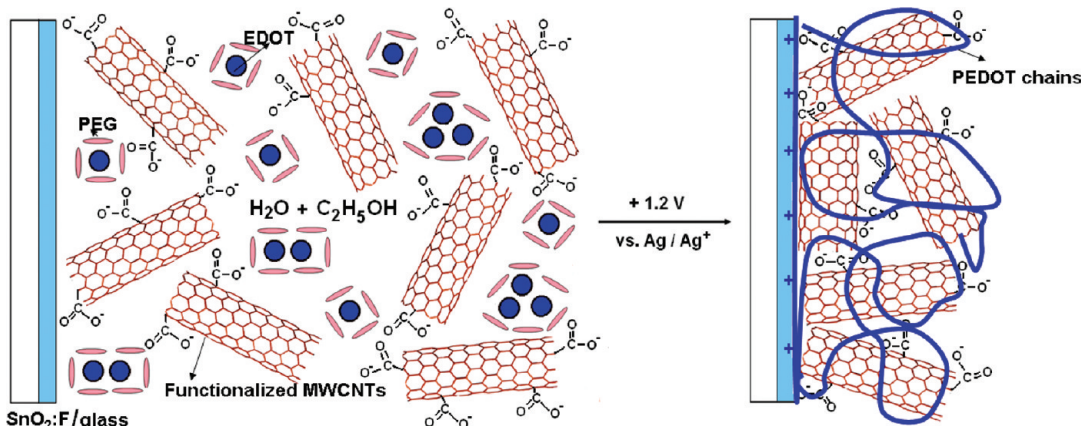


Figure 6. Schematic showing the formation of the PEDOT–MWCNT film from the solution containing EDOT, functionalized MWCNTs in a mixture of polyethylene glycol, water, and ethanol under a constant potential of +1.2 V.

PEDOT film, and this was also reflected in the disparity in the absorption spectra of the two films where the bipolaronic peak at ~ 800 nm characteristic of heavily doped and oxidized PEDOT was visible in the spectrum of the as-fabricated control PEDOT film, but it was not seen in the spectrum of the PEDOT–MWCNT film.²⁷ Its nonappearance is advantageous for the PEDOT–MWCNT electrode as it can reduce more easily than the control PEDOT film, and a higher optical density change is attainable at low reduction potentials. These spectra are shown in ref 27, and further discussions follow in section 3.5.

The density of states close to the Fermi level (corresponding to energy zero) can be viewed in Figure 4. No abrupt drop was observed in the density of states at zero binding energy, akin to that observed by Greczynski et al.³⁶ for PEDOT/PSS films in either of the two films under consideration. The calculated energy difference between the valence band and Fermi level is ~ 1.02 eV for the PEDOT–MWCNT film, which is lower than that of the control sample (1.6 eV). This hints at a lower band gap of the PEDOT–MWCNT film in comparison to that of the control PEDOT film, indubitably favoring an enhanced electrochromic contrast as a lower potential will suffice to induce electrochemical reduction and oxidation.

3.3. SEM, HRTEM, and AFM Studies.

SEM images of the PEDOT–MWCNT and the control PEDOT films are shown

in Figure 5. MWCNTs in the polymerization bath steer the formation of a predominantly fibrillar morphology of the PEDOT–MWCNT film by the virtue of their intrinsic tubular structure. Bundles of nanofibers of polymer enwrapping the MWCNTs, as illustrated by the schematic in Figure 6, are seen in Figure 5a and b. The diameter of these fibrils in the composites is inclusive of the diameter of MWCNTs. It is obvious that the MWCNTs serve as the nucleating site for polymer growth. This is further consolidated by the TEM image in Figure 7a. The schematic in Figure 6 shows that in the solution phase, the randomly distributed EDOT moieties are surrounded by the solubilizing agent polyethylene glycol and functionalized multiwalled carbon nanotubes. Upon application of the oxidation potential, the charged functionalized MWCNTs migrate to the anode, the monomer polymerizes, and a uniform film of nanotubular polymer grafted onto the functionalized MWCNTs is achieved. The generation of the carboxylic groups via oxidative treatment of the nanotubes through the opening of the MWCNT cap prior to its incorporation in the polymerizing formulation enables a direct bonding of the carboxylated tube portions to the polymer. The PEDOT–MWCNT film is also highly porous as pores with a diameter in the range of 40–90 nm are seen, and these provide an interconnected pore network conducive for rapid ion transport, which in turn imparts an enhanced redox response to the PEDOT–MWCNT film. In

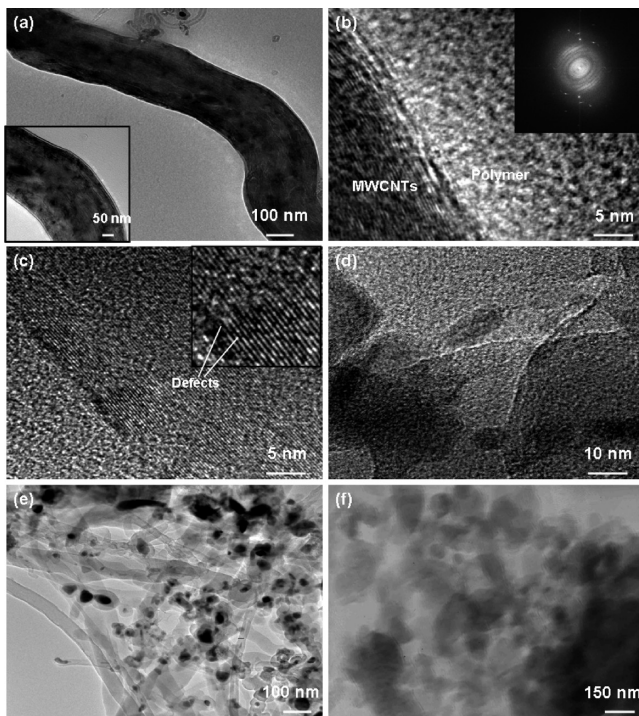


Figure 7. HRTEM micrographs of (a) the PEDOT-coated MWCNT, wherein the inner contours of the MWCNT are completely hidden. (b, c) The interface of PEDOT and a MWCNT; the amorphous polymer and the walled structure of the MWCNT are clearly distinguishable; the inset of (b) shows that the SAED pattern of the nanotubes and that of (c) shows that the defects in MWCNTs caused by functionalization. (d) Overlapping tubes of PEDOT–MWCNTs; (e) low-magnification TEM image of the PEDOT–MWCNT film showing dominant nanotubular structure; (f) granular structure of control PEDOT.

contrast, the morphology of the control PEDOT film (Figure 5c) consists of closely packed large micrometer-sized particles of well-defined shapes spread uniformly all across the specimen.

The TEM micrograph in Figure 7a reveals a uniform coating of the polymer on the MWCNT, and one such entity from the PEDOT–MWCNT film is depicted therein. The inner contours of the multiwalled nanotubes (diameter $\sim 200\text{--}270\text{ nm}$) are completely hidden due to the effective wrapping by PEDOT chains, and even the magnified view in the inset does not show the finer features of the ensconced MWCNTs. The HRTEM image in Figure 7b, however, provides an exquisite view of the interface of MWCNTs characterized by striations showing the walls of the nanotubes and the granular texture of the polymer matrix. The SAED (inset of Figure 7b) shows diffuse rings which correspond to the amorphous PEDOT, and the bright spots superimposed on the rings are due to the crystalline functionalized MWCNTs. The defects created in the MWCNTs by functionalization are also seen in the micrograph (Figure 7c). Crisscross PEDOT–MWCNT nanotubes in Figure 7d show the homogeneous mixing of the two components of the composite. That the tubular and not the particulate structure preponderates in the PEDOT–MWCNT film is confirmed from the low-magnification image of the film in Figure 7e, wherein overlapping polymer–MWCNT tubular shapes, with diameters in the range of 50–80 nm oriented parallel to the substrate, are distinctly seen. The aspect ratio of the PEDOT–MWCNTs lies in the range of 400–500. On the other hand, the TEM image of the control PEDOT film (Figure 7f) shows mingling grains with no distinct grain boundaries; the diffuse grains indicate an amorphous structure.

Noncovalent interactions between the MWCNTs and the surrounding polymer matrix allowed the formation of a uniform, homogeneous film and complete coverage of the substrate during electropolymerization with minimum defect/pinhole density. This was achieved by means of an optimal level of functionalization of MWCNTs; it was adequate enough to allow the formation of a homogeneous suspension of the MWCNTs in the water–ethanol electropolymerization bath (wherein the dispersed phase remained in solution without separating out; separation takes place when the functionalization level is too low, and no electropolymerization occurs even if the bath is continuously agitated during electropolymerization), and at the same time, it was low enough to not introduce too many defects in the nanotube lattice. If the nanotubes had been completely destroyed during functionalization, the film microstructure would have consisted of particles instead of tubular shapes.

The significant disparity in the microstructures of the PEDOT–MWCNT and the control PEDOT film was also observed through AFM images in Figure 8. Figure 8a displays the MWCNTs coated by the polymer chains, which significantly increase their original diameter ($\sim 150\text{ nm}$), concomitant with our findings in an earlier report.²⁷ The dark and the bright contours are suggestive of the porosity present in the film, whereas in the control PEDOT film, the structure is constituted mainly of micrometer-sized discs. Upon comparing the undulations in the height profile displayed in Figure 8c and c', it is evident that the PEDOT–MWCNT film structure is more uniform as compared to the control PEDOT film.

3.4. CV, LSV, and EIS Investigations. The redox chemistry of the films was examined by switching the potential of the films between -1 to $+1\text{ V}$ in a nonaqueous $1\text{ M LiClO}_4\text{--PC}$ electrolyte at 5 mV s^{-1} (Figure 9). The PEDOT–MWCNT film shows an anodic peak at $+0.01\text{ V}$ corresponding to perchlorate ion insertion or doping, and a cathodic peak in the reverse scan due to dedoping appears at -0.56 V (Figure 9a). While a distinct reduction peak is also seen in the control PEDOT film, the corresponding anodic peak was not seen. The weak shoulder seen at $+0.65\text{ V}$ in the voltammograms of both films is due to cation extraction from the polymer film, and it is not seen in the reverse sweep because of the differing rate of the two processes. The maximum cathodic (j_{cmax}) and anodic (j_{amax}) peak current densities observed in the PEDOT–MWCNT film are 0.33 and 0.17 mA cm^{-2} , whereas in the control PEDOT film, only a j_{cmax} of 0.20 mA cm^{-2} is seen. Furthermore, the charge density for the perchlorate ions inserted and extracted in the PEDOT–MWCNT film are 1.18 and 0.96 mC cm^{-2} , respectively, in comparison to 0.98 and 0.78 mC cm^{-2} for the control sample, implying a larger charge storage capacity available to the PEDOT–MWCNT film. The higher redox activity of the PEDOT–MWCNT film indicates a strong interaction between MWCNTs and the polymer,^{25,26} which is a result of an open structure and the higher surface area due to the nanotubular structure. Additionally, MWCNTs provide carrier-transporting channels through them due to their high aspect ratio.¹⁷ The greater value of the diffusion coefficient calculated from the Randles–Sevcik equation of composite films ($D = 2.9 \times 10^{-10}\text{ cm}^2\text{ s}^{-1}$) in comparison to that of the control PEDOT film ($D = 1.08 \times 10^{-10}\text{ cm}^2\text{ s}^{-1}$) further exemplified the ease of ion transport though the bulk of the film during oxidation of the PEDOT–MWCNT film. The influence of repeated cycling between oxidized and reduced states on the redox response of the PEDOT–MWCNT film is shown in Figure 9b. The shape of the voltammogram is not obscured much even after 2000 cycles, but the

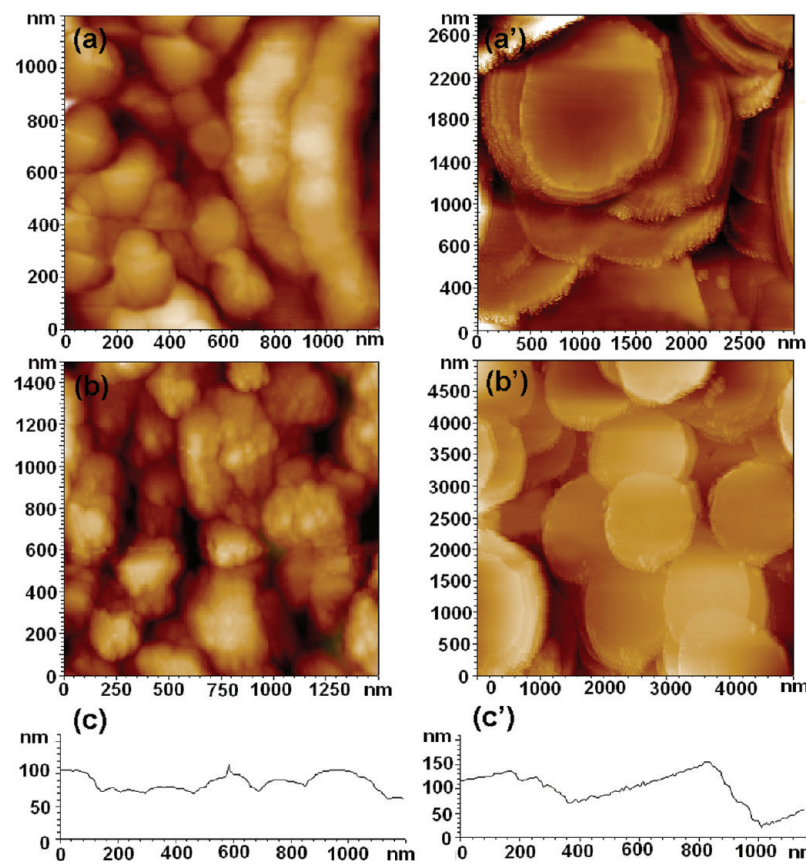


Figure 8. High- and low-magnification AFM images of (a, b) PEDOT–MWCNT, (a', b') control PEDOT films, and the height profiles of (c) PEDOT–MWCNT and (c') control PEDOT films recorded over a width of $\sim 1.2 \mu\text{m}$.

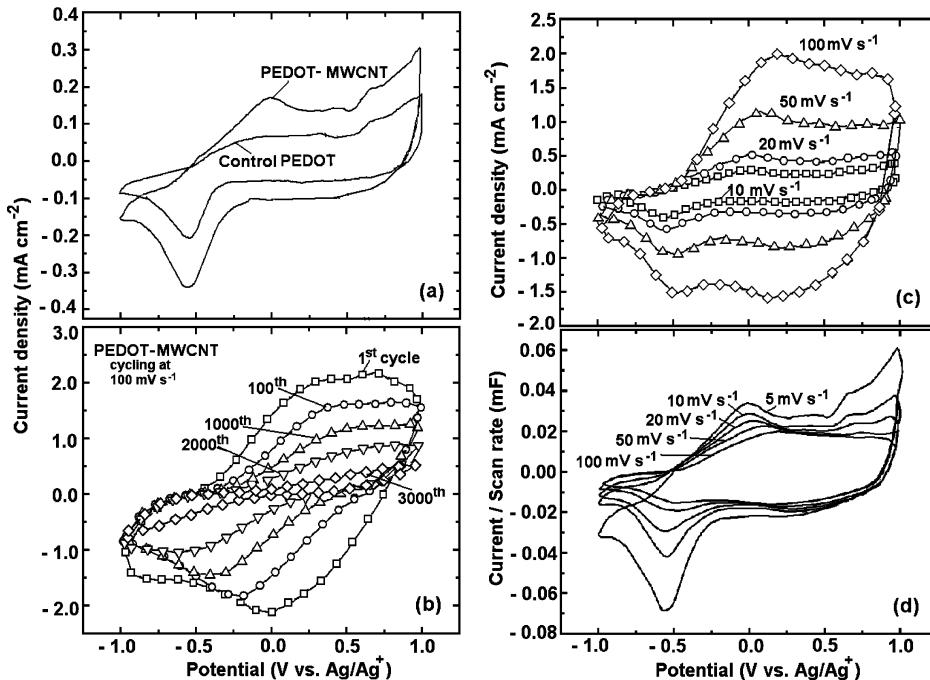


Figure 9. Cyclic voltammograms of (a) PEDOT–MWCNT and control PEDOT films recorded at 5 mV s⁻¹, (b) PEDOT–MWCNT film depicting its cycling response up to 3000 cycles at a constant rate of 100 mV s⁻¹, (c) PEDOT–MWCNT film as a function of scan rates, 10, 20, 50, and 100 mV s⁻¹, and (d) voltammetric capacitance versus potential for PEDOT–MWCNT at different scan rates, all in 1 M LiClO₄–PC electrolyte.

electrochemical activity loss with cycling is perceptible from the shrinkage of the area under the curve in Figure 9b, especially after 3000 cycles. The charge capacity during ingress and egress of the ion in initial cycles is 2.9 and 2.2 mC cm⁻², respectively, whereas after 3000 cycles, these

diminish to 0.78 and 0.48 mC cm⁻², respectively. For the control film, the charge capacities were even lower, 1.6 and 2.0 mC cm⁻², and these reduced to 0.68 and 0.12 mC cm⁻², again affirming the superior electrochemical activity of the PEDOT–MWCNT film.

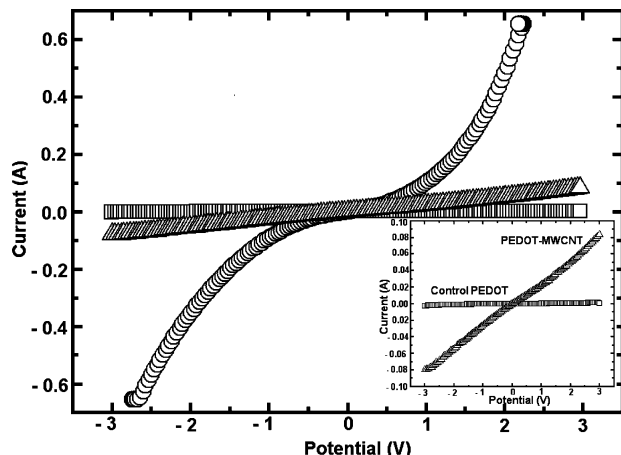


Figure 10. I – V characteristics of functionalized MWCNTs (○), PEDOT–MWCNT (△), and control PEDOT films (□); the inset is the magnified view to illustrate higher currents achieved in PEDOT–MWCNT in comparison to those in control PEDOT films.

The CV plots of the PEDOT–MWCNT as a function of scan rate are shown in Figure 9c. The figure clearly shows a nearly linear relationship between the anodic/cathodic current density maxima and the scan rate, suggesting the presence of surface-confined redox active states in the PEDOT–MWCNT film. The capacitive character of the film also appears to increase with scan rate, and this has been illustrated by plotting the voltammetric capacitance of the PEDOT–MWCNT film (Figure 9d). With increasing scan rate, the peak potential shows a positive shift during oxidation, while no major shift is visible during the reverse scan, which reflects the presence of the uncompensated resistance in the polymer during the oxidation process.³⁷

The I – V characteristics of functionalized MWCNTs, PEDOT–MWCNT, and control PEDOT are shown in Figure 10. The conductivity of functionalized MWCNTs was determined to be 40.6 mS cm^{-1} by assuming a linear current–voltage dependence. For the composite PEDOT–MWCNT film, it was found to be 5.04 mS cm^{-1} , which is higher than that of the PEDOT doped with traditional dopant ions in the literature.³⁸ Higher values of conductivities have been reported for carbon nanotubes in the literature,^{39,40} but because they are randomly arranged and not aligned arrays here and perhaps due to a high functionalization level, the conductivity is lower than expected. The conductivity of the control PEDOT film was found to be as low as 0.084 mS cm^{-1} . The PEDOT–MWCNT film's conductivity was 60 times higher than that of the control PEDOT film, which validates that the interfacial bonding between the polymer and MWCNT is strong and capable of mediating facile charge transfer at the PEDOT/MWCNT interface and its subsequent delocalization in the PEDOT–MWCNT film. In a previous report,⁴¹ a sheet resistance of about $1 \text{ K}\Omega \text{ cm}^{-2}$ was achieved in transparent conductive patterns of the PEDOT/PSS–SWCNT. Here, the bulk resistance of the PEDOT–MWCNT is higher ($192.9 \Omega \text{ cm}^{-2}$), but it is higher by several orders for control PEDOT ($11514 \Omega \text{ cm}^{-2}$).

The Z' versus Z'' response of PEDOT–MWCNT and control PEDOT films recorded under different dc conditions is shown in Figure 11a and b. Interpretation of charge-transfer and capacitive characteristics of the films has been provided elsewhere.²⁷ Here, the ionic conductivity of the films at different potentials (at intervals of 0.25 V) has been extracted from the Nyqvist plots using the diameter of the impedance arc, which is in accordance with the method proposed for ionic conductivity measurements performed on polypyrrole samples by Pickup et

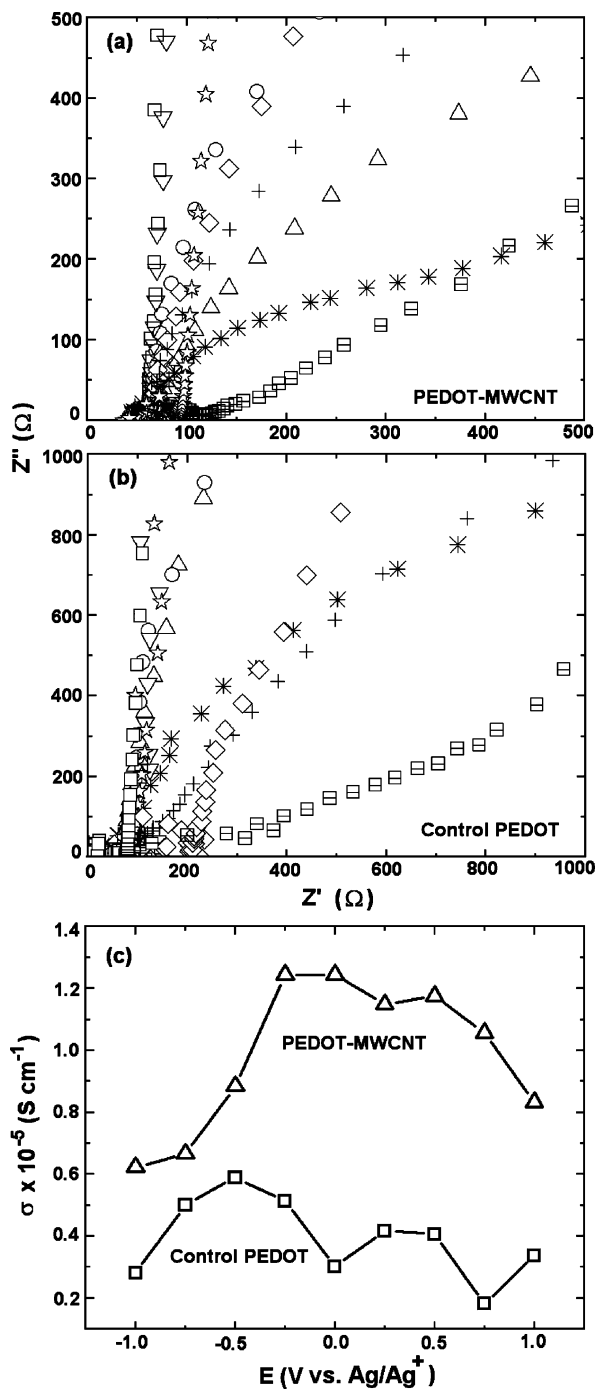


Figure 11. (a) Nyqvist plots of (a) PEDOT–MWCNT and (b) control PEDOT films recorded under different dc potentials of $+1.0$ (box with slash), $+0.75$ (◊), $+0.5$ (☆), $+0.25$ (▽), 0 (□), -0.25 (○), -0.5 (△), -0.75 (*) and -1.0 (+) V in 1 M LiClO_4 in propylene carbonate. (c) Ionic conductivity (derived from a and b) as a function of applied potential of PEDOT–MWCNT (△) and control PEDOT (□) films.

al.^{42–44} The authors observed that this treatment is extendable to other conducting polymers and yields fairly accurate conductivities. The ionic conductivity of PEDOT–MWCNT (Figure 11c) is much larger than that of control PEDOT films over the entire potential range of $+1.0$ to -1.0 V under consideration. Evidence for the relative ease of ion percolation and diffusion in the PEDOT–MWCNT composite as compared to that in the control PEDOT film is visible in this plot. For the PEDOT–MWCNT film, ionic conductivity was found to increase with decreasing potential until -0.25 V , and upon further reduction, the conductivity decreased. It is apparent that the film, in addition

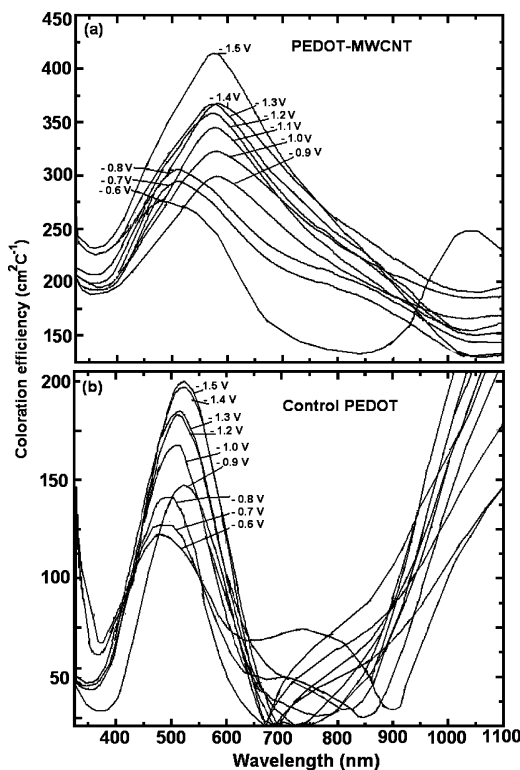


Figure 12. Coloration efficiency plots of (a) PEDOT–MWCNT and (b) control PEDOT films as a function of wavelength under different bias potentials varying from −0.6 to −1.5 V in steps of 0.1 V; the optical state under −0.5 V has been taken as the reference.

to being efficient at anion exchange with the electrolyte, also acts as a cation exchanger since conductivity is retained and does not decline drastically in the reduction regime, as electronic conductivity does in poly(3,4-alkyldioxythiophenes).⁴⁵ The largest ionic conductivity of 1.24×10^{-5} S cm⁻¹ attained by PEDOT–MWCNT, however, is 10 times lower than reported for polypyrrole doped with perchlorate ions,⁴⁴ and this we attribute to the intrinsic differences in the two polymers. In the case of the control PEDOT film, the trend shows that cations dominate the ion-transport process as conductivity under negative potentials is higher than that observed at positive potentials. The overall conductivity profile for both control PEDOT and PEDOT–MWCNT shows that only the type of charge carriers are changing with applied potential, and this is responsible for the observed differential in ionic conductivity of the films in their oxidized and reduced states. This is in stark contrast to the well-reported electronic conduction of PEDOT, wherein the electronic conductivity increases by 4 orders of magnitude; the film transforms from an insulating to almost metallic state, ongoing from negative to positive bias.⁴⁵ It is therefore apparent that in addition to being an electron conductor, the PEDOT–MWCNT film is an ion conductor as well, irrespective of its redox state.

3.5. UV–Vis Spectrophotometry and Chronoamperometry. The wavelength dependence of the coloration efficiency (η), defined as the change in the optical density (ΔOD) for the charge (q) consumed per unit electrode area (A),⁴⁶ is shown in Figure 12.

$$CE(\eta) = \Delta OD(\lambda)/(q/A) \quad (1)$$

The reference voltage was fixed at −0.5 V for both films. For the PEDOT–MWCNT film, the coloration efficiency shows

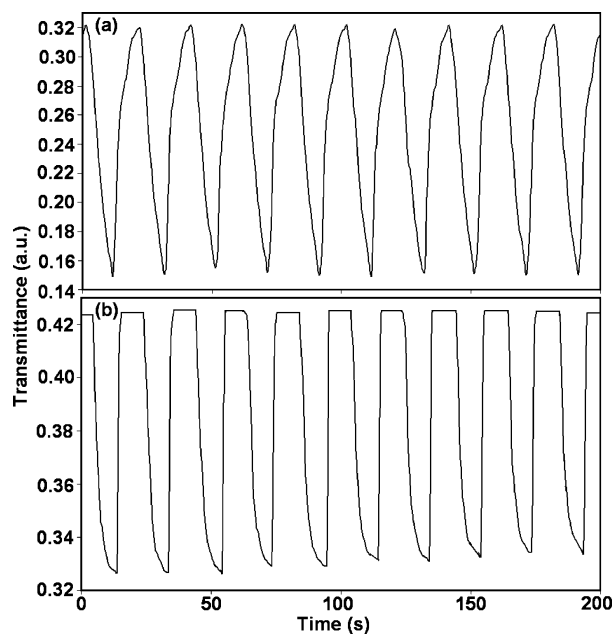


Figure 13. Variation of transmittance at a monochromatic wavelength of 632.8 nm as a function of time for (a) PEDOT–MWCNT and (b) control PEDOT films under a square wave dc potential of ±1.5 V at a frequency of 0.05 Hz.

its maximum of $414 \text{ cm}^2 \text{ C}^{-1}$ ($\lambda_{\max} = 575 \text{ nm}$) at −1.5 V. In this film, the coloration efficiency maximum $CE_{\max}(\lambda)$ shows a red shift from 511 to 575 nm as the potential is increased from −0.8 onward up to −1.5 V in steps of 0.1 V. However, in the control film, $CE_{\max}(\lambda)$ shows variation at −0.9 V with $CE_{\max}(\lambda)$ at 523 nm, whereas the remaining potential's CE_{\max} is seen in the 498–512 nm range, which shows a positive shift with an increase in potential. The maximum coloration efficiency observed by the control PEDOT film is $201 \text{ cm}^2 \text{ C}^{-1}$ ($\lambda_{\max} = 520 \text{ nm}$) at −1.5 V. At lower potentials of −0.6 and −0.7 V, CE shows broad peaks centered at approximately 757 ($\eta = 98 \text{ cm}^2 \text{ C}^{-1}$) and 735 nm ($\eta = 43 \text{ cm}^2 \text{ C}^{-1}$) after λ_{\max} . Here, either the impact of the doping level on the electronic structure or the bond length alteration with the change in potential can possibly be the reason for the different CE_{\max} with different bias potentials. Since the band gap of conducting polymers is influenced by several factors like mesoscopic ordering, conjugation length, bond length, doping level, conformational changes,⁴⁷ and so forth, these affect the optical density and hence the coloration efficiency. The maximum value of coloration efficiency shown by the PEDOT–MWCNT film ($\eta = 414 \text{ cm}^2 \text{ C}^{-1}$, $\lambda_{\max} = 575 \text{ nm}$, $E = -1.5 \text{ V}$) is almost double that observed by the control film ($\eta = 201 \text{ cm}^2 \text{ C}^{-1}$, $\lambda_{\max} = 520 \text{ nm}$, $E = -1.5 \text{ V}$). In the visible region, the coloration efficiency is larger for the PEDOT–MWCNT film and does not drop to 0 at 700 nm as it does in the control PEDOT film. The observed coloration efficiency is slightly higher than that of neat PEDOT films electrodeposited earlier in organic media as reported by Gaupp et al.⁴⁸ ($\eta = 183 \text{ cm}^2 \text{ C}^{-1}$) and more than that obtained for some PEDOT derivatives formed to enhance coloration efficiency.⁴⁹ However, P(BEDOT–MEHB) by Sonnenz et al.⁵⁰ and a perfluoroalkanoate-substituted PEDOT⁵¹ show very large coloration efficiencies of 680 and 586 cm² C⁻¹. It is very clear that the PEDOT–MWCNT film shows a higher coloration efficiency at lower operating voltages, which can be effectively translated to longer operational device lifetimes when used in prototype electrochromic devices.

The color–bleach characteristics of the films recorded at 632.8 nm under ±1.5 V at an optimized frequency of 0.05 Hz

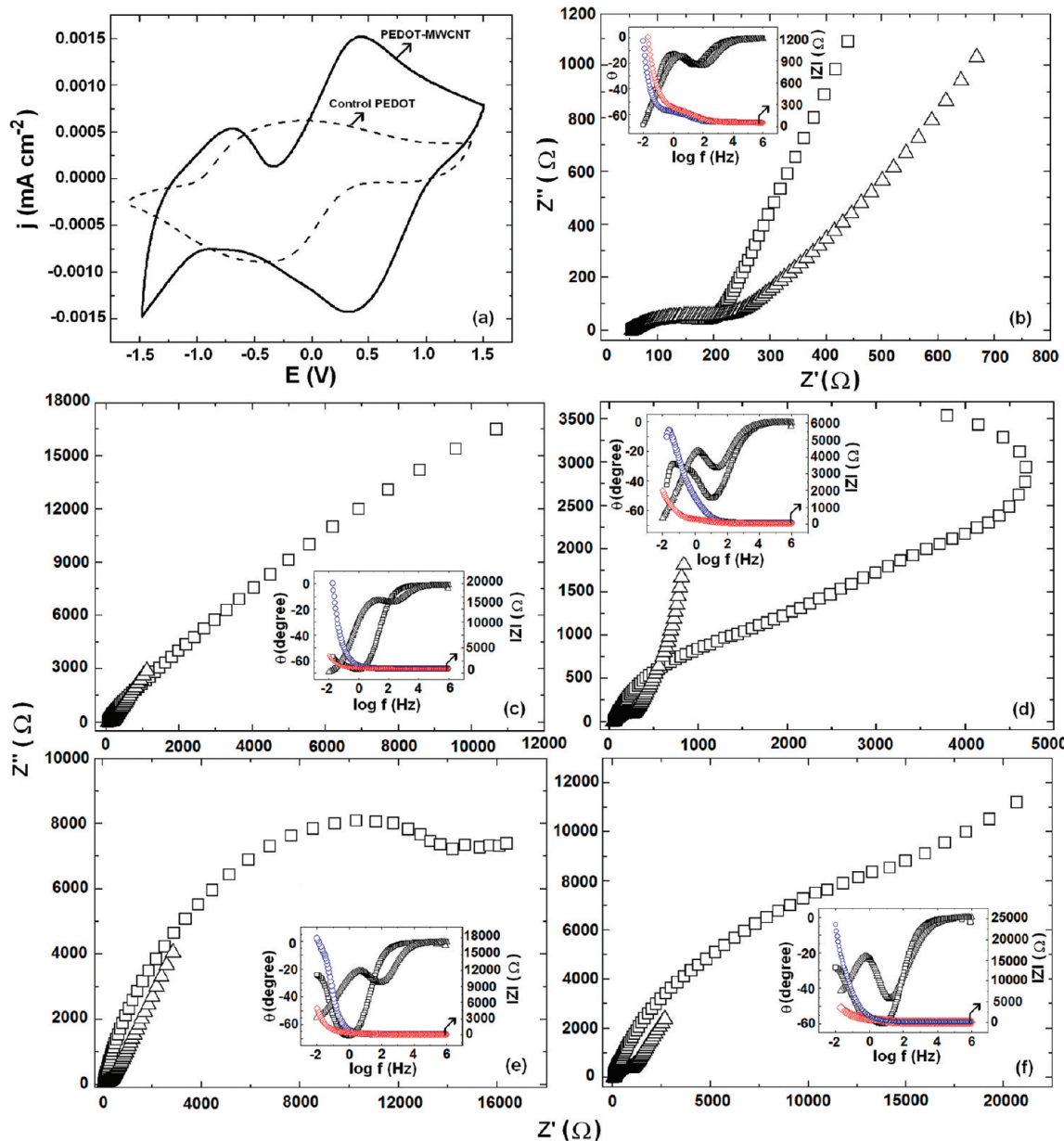


Figure 14. (a) Cyclic voltammograms of PEDOT–MWCNT/PB (—) and control PEDOT/PB (---) devices recorded at 100 mV s^{-1} and Nyquist plots of PEDOT–MWCNT/PB (Δ) and control PEDOT/PB (\square) devices recorded under an ac amplitude of 20 mV at different dc potentials, (b) 0, (c) -1.0 , (d) $+1.0$, (e) -1.5 , and (f) $+1.5 \text{ V}$. Insets show the corresponding Bode plots, θ versus $\log f$ of PEDOT–MWCNT/PB (Δ) and control PEDOT/PB (\square) and $|Z|$ versus $\log f$ of PEDOT–MWCNT/PB (\diamond) and control PEDOT/PB (\circ) devices.

is shown in Figure 13. The high current-carrying capacity of the PEDOT–MWCNT owing to the dominant nanotubular morphology is reflected in switching times as well. The switching kinetics is examined by evaluating the time taken for a 90% transmission change of the total optical contrast for the films of the same thickness and geometric area. Though the bleaching times of the two do not differ largely (PEDOT–MWCNT $\sim 2.8 \text{ s}$ and PEDOT $\sim 3.2 \text{ s}$), their coloration times show that the PEDOT–MWCNT film colors more rapidly. The time required by PEDOT–MWCNT to acquire a dark blue state is 7.0 s , whereas the control film takes nearly double that time to turn blue (its total contrast being 59% of that shown by PEDOT–MWCNT). The better porosity and the larger effective surface area afforded by the nanotubular morphology of the PEDOT–MWCNT allows faster ion movement in the film, thus manifesting in faster color–bleach kinetics. The pores in the PEDOT–MWCNT film permit better adsorption of the electrolytic solution, which enables easier access of electrolyte ions

with the electrochemically active sites on the electrode, and therefore, the amplitude of optical contrast is enhanced.

3.6. Electrochemical Response of Devices Based on PEDOT–MWCNT and Control PEDOT Films. Unlike conventional dopants, which are essentially electrolyte salt anions, functionalized MWCNTs offer many advantages which improve the electrochemical activity of the conducting polymer. MWCNTs allow electron transport as they are intrinsic electron conductors, and if the interface between the polymer and MWCNT is strong (as it is herein, which is distinctly seen in the TEM images), the transport of electrons will be advanced, movement of electrons will not be confined to the polymer chains only (as happens in the case of PEDOT doped by conventional salt anions), but the charges can diffuse unobstructed through the PEDOT/MWCNT interface. These effects have been quantitatively realized by comparing the electrochemistry of electrochromic devices formed from PEDOT–MWCNT and control PEDOT layers. The cyclic voltammogram of the PEDOT–MWCNT

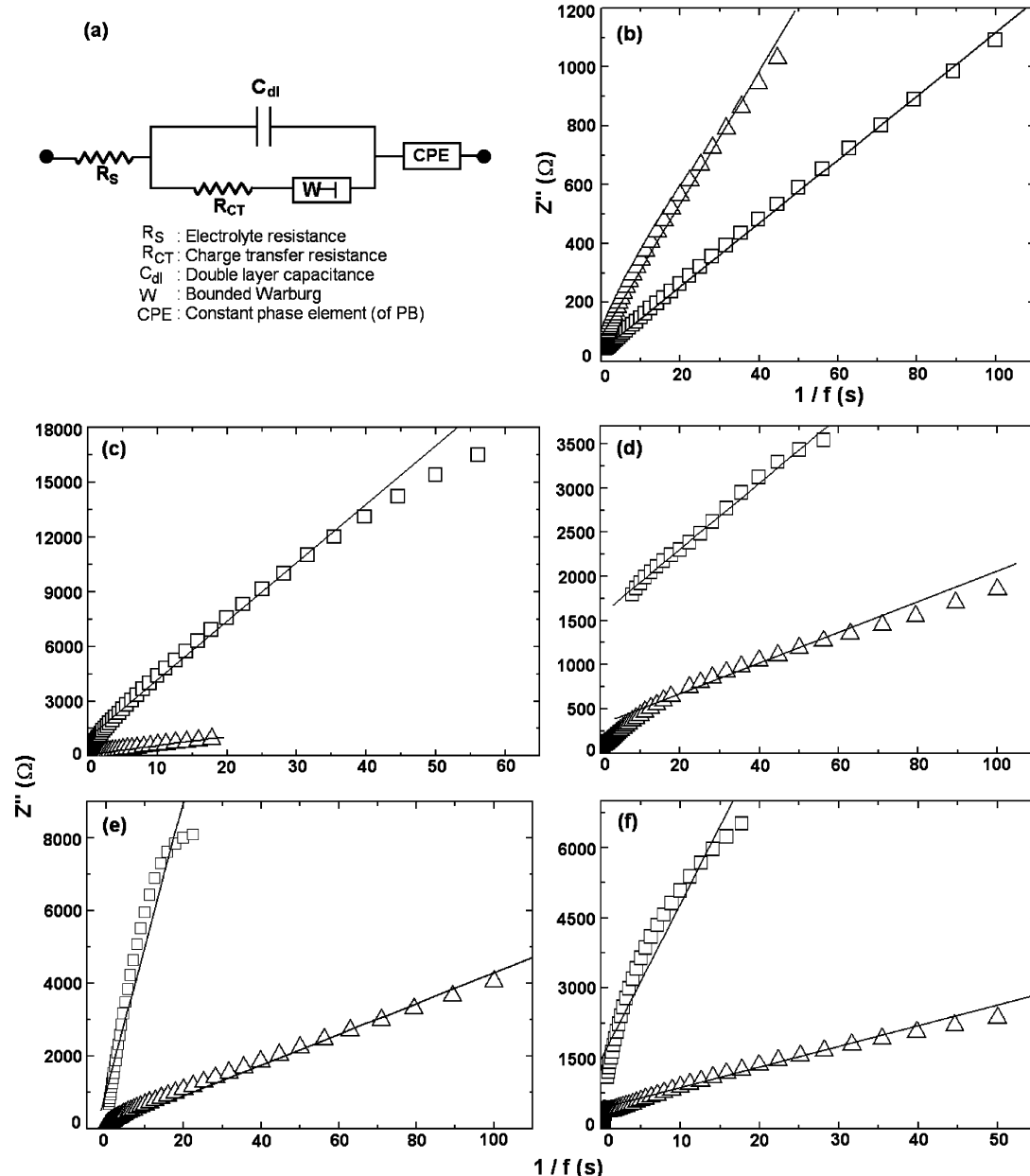


Figure 15. (a) Randles equivalent circuit used for fitting the experimental data in Figure 14 and imaginary impedance versus the reciprocal of frequency plots in the low-frequency region for PEDOT–MWCNT/PB (Δ) and control PEDOT/PB (\square) devices at different dc potentials, (b) 0, (c) -1.0 , (d) $+1.0$, (e) -1.5 , and (f) $+1.5$ V. Lines show the corresponding linear fits.

device (Figure 14a) shows an anodic peak at $+0.41$ V due to triflate insertion, and the cathodic peak is seen at $+0.31$ V. An additional peak seen at -0.72 V in the anodic branch in the reverse sweep is ascribed to charge trapping.⁵² The control PEDOT film based device shows broad oxidation and reduction waves with much lower current density maxima. It is known that the PEDOT–MWCNT film can support high currents due to strong C–C bonds,³⁹ and this too contributes to larger current densities. The Z versus Z' curves are shown in Figure 14 and the insets display the corresponding Bode plots for the two devices under different dc conditionings (applied to the PEDOT film in both devices). The equivalent circuit displayed in Figure 15a gave acceptable fits over the entire frequency range of $\sim 10^6$ – 0.01 Hz. Irrespective of the applied potential, the impedance response of the PEDOT–MWCNT device is similar to that of the control PEDOT device in the high-frequency region, but the responses are strikingly different in the low-frequency regime, and this difference is more apparent from

the corresponding Bode plots. The amplitude of the impedance curve is much larger for the control PEDOT based device as compared to the PEDOT–MWCNT device under all dc potentials except for the zero dc bias condition (as can be seen from the $|Z|$ versus $\log f$ plots in the insets of Figure 14), which is evidence for the fact that during oxidation and reduction, charge transfer and capacitive and diffusion processes are more obstructed in the control PEDOT device. This is also reflected in the lower magnitudes of charge-transfer resistance (R_{CT}) and higher values of Y_0 for the PEDOT–MWCNT electrode, the latter being a direct measure of how easily ions ingress and egress.

Table 2 furnishes a comparison of the electrochemical parameters for the two devices. The dominant nanotubular morphology and the porous structure of the PEDOT–MWCNT film in comparison to the conventional particulate structure of the control PEDOT film and the ability of MWCNTs to allow efficient charge propagation across the PEDOT/MWCNT in-

TABLE 2: Electrochemical Impedance Spectroscopy Results for PEDOT–MWCNT and Control PEDOT Based Devices, Obtained by Fitting the Experimental Data in the Model Shown in Figure 15a and C_D from Figure 15b–f

applied E (V)	R_{CT} (Ω)		Y_0 (S ($s^{1/2}$))		C_D (mF cm^{-2})	
	PEDOT–MWCNT	Control PEDOT	PEDOT–MWCNT	control PEDOT	PEDOT–MWCNT	control PEDOT
0	82.0	90.0	2.7×10^{-3}	6.0×10^{-3}	5.5	6.5
-1.0	100.0	116.0	2.3×10^{-3}	0.14×10^{-3}	4.2	0.16
-1.5	100.0	6000.0	0.82×10^{-3}	0.24×10^{-3}	5.03	0.13
+1.0	10.0	700.0	15.0×10^{-3}	0.36×10^{-3}	7.65	1.41
+1.5	21.0	600.0	1.2×10^{-3}	0.96×10^{-3}	4.0	0.16

terface are responsible for the easier ion transfer at the PEDOT–MWCNT electrode/electrolyte interface and faster diffusion rate of solvated lithium ions or triflate ions within the PEDOT–MWCNT film. Further, the PEDOT–MWCNT electrode has a lower R_{CT} and a higher Y_0 in its oxidized state (+1.0 and +1.5 V) (Figure 14 d and f) as compared to a higher R_{CT} and lower Y_0 in its reduced state (-1.0 and -1.5 V) (Figure 14c and e), which implies that doping by counterions is more facile than dedoping. This is natural as the doped state of the film is electronically conducting and therefore has more electrochemically accessible surface sites, whereas in the dedoped state, the film tends to be insulating, and as a consequence, charge-transfer and capacitive characteristics of PEDOT–MWCNT are affected. In the as-fabricated state (Figure 14b), under zero dc bias, for both PEDOT–MWCNT and control PEDOT based devices, the finite length Warburg diffusion line is inclined to 90°, and it is inclined more for the control PEDOT device, which is typically a capacitive behavior. The linear variation of imaginary impedance with the reciprocal of frequency in the low-frequency region shown in Figure 15 yielded the diffusional pseudocapacitance ($C_D = 1/\omega Z''$) of the electrodes during oxidation and reduction. As an illustrative example, the low-frequency capacitance of the PEDOT–MWCNT electrode under +1.0 V (oxidation) is 10 mF cm^{-2} , and that of control PEDOT electrode under the same potential is 1.4 mF cm^{-2} , which again demonstrates that the microstructure of the PEDOT–MWCNT film is responsible for the relatively easier charging of the electrode by electrolyte anions. The capacitances (C_D) obtained from Figure 15 have greater magnitudes for the PEDOT–MWCNT based device than those for the control PEDOT device, indicative of the superior charging–discharging ability of the former. Owing to the inherent electron-conducting nature of CNTs and as they also provide multiple redox active sites due to functionalization, both electron and ion transport through the PEDOT–MWCNT film are facilitated, be it oxidation (or bleaching) and reduction (or coloration). Such effects are not realized in the device based on the control PEDOT film, and therefore, its electrochemical activity is lower than that of the PEDOT–MWCNT based device.

4. Conclusions

Poly(3,4-ethylenedioxythiophene)-coated functionalized multiwalled carbon nanotubes fabricated as composite thin films using electropolymerization showed superior redox activity and larger coloration efficiency in the photopic region in comparison to control PEDOT films. Functionalized MWCNTs in addition to serving as dopant ions for the positively charged polymer layer are also responsible for the formation of films composed of interlinked bundles of nanotubular structures and porous networks, which promote ion/electron transfer at the PEDOT–MWCNT/electrolyte interface and allow electron diffusion at the PEDOT/MWCNT interface by virtue of strong electrostatic interaction between the functionalized carbons and the polymer.

Electrochromic devices based on PEDOT–MWCNT and control PEDOT films during oxidation and reduction showed a lower charge-transfer resistance, a higher diffusional capacitance, and a significantly reduced amplitude of impedance arc over a wide frequency range, thus making it evident that capacitive and transport phenomena proceed unencumbered in the PEDOT–MWCNT film. PEDOT–MWCNT films afford efficient charge propagation during redox switching, which cannot be realized in PEDOT films doped by conventional salt anions.

Acknowledgment. The authors are indebted to NPL for the financial support. One of the authors, S.B., acknowledges the University Grants Commission (UGC) for a senior research fellowship. We thank Dr. Dinesh Dewa, Department of Physics, IIT Kanpur, for AFM measurements, Dr. Chhotey Lal, National Physical Laboratory, for experimental help, and Dr. S.T. Lakshmikumar, National Physical Laboratory, for his guidance and encouragement.

Supporting Information Available: X-ray diffraction patterns, SEM images, and TEM micrographs. This material is available free of charge via the Internet at <http://pubs.acs.org>.

References and Notes

- Iijima, S. *Nature* **1991**, *354*, 56.
- Ajayan, P. M.; Zhou, O. Z. In *Carbon Nanotubes: Synthesis, structure, properties and applications*; Dresselhaus, M. S., Dresselhaus, G., Avouris P., Eds.; Springer-Verlag: Berlin, Germany, 2000; Chapter 13.
- Grimes, C. A.; Mungle, C.; Kouzoudis, D.; Fang, S.; Eklund, P. C. *Chem. Phys. Lett.* **2000**, *319*, 460.
- Treacy, M. M. J.; Ebbesen, T. W.; Gibson, J. M. *Nature* **1996**, *381*, 628.
- Breuer, O.; Sundararaj, U. *Polym. Compos.* **2004**, *25*, 630.
- Szleifer, I.; Rozen, R. Y. *Polymer* **2005**, *46*, 7803.
- Xie, X. L.; Mai, Y. W.; Zhou, X. P. *Mater. Sci. Eng. Res.* **2005**, *49*, 89.
- Downs, C.; Nugent, J.; Ajayan, P. M.; Duquette, D. J.; Santhanam, K. S. V. *Adv. Mater.* **1999**, *11*, 1028.
- Frackowiak, E.; Khomenko, V.; Jurewicz, K.; Lota, K.; Beguin, F. *J. Power Sources* **2006**, *153*, 413.
- Zhou, Q.; Wood, J. R.; Wagner, H. D. *Appl. Phys. Lett.* **2001**, *78*, 1748.
- de Heer, W. A.; Chatelain, A.; Ugarte, D. A. *Science* **1995**, *270*, 1179.
- Alig, I.; Skipa, T.; Engel, M.; Lellinger, D.; Pegel, S.; Potschke, P. *Phys. Status Solidi B* **2007**, *4223*.
- McNally, T.; Potschke, P.; Halley, P.; Murphy, M.; Martin, D.; Bell, S. E. J.; Brennan, G. P.; Bein, D.; Lemoine, P.; Quinn, J. P. *Polymer* **2005**, *46*, 8222.
- Markovic, M. G.; Martisons, J. G.; Cervini, R.; Simon, G. P.; Fredericks, P. M. *Chem. Mater.* **2006**, *18*, 6258.
- Lu, X.; Chao, D.; Zheng, J.; Chen, J.; Zhang, W.; Wei, Y. *Polym. Int.* **2006**, *55*, 945.
- Ramirez, A. P. *Bell Lab. Tech. J.* **2005**, *10*, 171.
- Pradhan, B.; Batabyal, S. K.; Pal, A. J. *Appl. Phys. Lett.* **2006**, *88*, 093106.
- Avouris, P.; Appenzeller, J. *Ind. Phys.* **2004**, *10*, 18.
- Islam, M. F.; Rojas, E.; Bergey, D. M.; Johnson, A. T.; Yodh, A. G. *Nano Lett.* **2003**, *3*, 269.
- Liu, Y.; Taylor, S.; Li, H. P.; Fernando, K. A. S.; Qu, L. W.; Wang, W.; Gu, L. R.; Zhou, B.; Sun, Y. P. *J. Mater. Chem.* **2003**, *14*, 1527.

- (21) Liu, J.; Rinzler, A. G.; Dai, H.; Hafner, J. H.; Bradley, R. K.; Boul, P. J.; Lu, A.; Iverson, T.; Shelimov, K.; Huffman, C. B.; Rodriguez-Macias, F.; Shon, Y. S.; Lee, T. R.; Colbert, D. T.; Smalley, R. E. *Science* **1998**, *280*, 1253.
- (22) Hughes, M.; Chen, G. Z.; Shaffer, M. S. P.; Fray, D. J.; Windle, A. H. *Chem. Mater.* **2002**, *14*, 1610.
- (23) Bandaru, P. R.; In *Carbon Nanotubes: Multifunctional Materials*; Somani, P. R., Umeno, M., Eds.; Applied Science Innovations Pvt. Ltd: India and Chuba, Japan, 2009; Chapter 5, pp 114.
- (24) Chen, G. Z.; Shaffer, M. S. P.; Coleby, D.; Dixon, G.; Zhou, W.; Fray, D. J.; Windle, A. H. *Adv. Mater.* **2000**, *12*, 522.
- (25) Wu, M.; Snook, G. A.; Gupta, V.; Shaffer, M.; Fray, D. J.; Chen, G. Z. *J. Mater. Chem.* **2005**, *15*, 2297.
- (26) Peng, C.; Jin, J.; Chen, G. Z. *Electrochim. Acta* **2007**, *53*, 525.
- (27) Bhandari, S.; Deepa, M.; Srivastava, A. K.; Lal, C.; Kant, R. *Macromol. Rapid Commun.* **2008**, *29*, 1959.
- (28) Randriamahazaka, H.; Noel, V.; Chevrot, C. *J. Electroanal. Chem.* **1999**, *472*, 103.
- (29) Deepa, M.; Bhandari, S.; Kant, R. *Electrochim. Acta* **2009**, *54*, 1292.
- (30) Konyushenko, E.; Stejskal, J.; Trchova, M.; Hradil, J.; Kovarova, J.; Prokes, J.; Cieslar, M.; Hwang, J.-Y.; Chen, K.-H.; Sapurina, I. *Polymer* **2006**, *47*, 5715–5723.
- (31) Bellamy, L. J. *The Infra-red spectra of complex molecules*; John Wiley and Sons, Inc.: New York, 1954; Chapter 10, p 139.
- (32) Kakade, B. A.; Pillai, V. K. *J. Phys. Chem. C* **2008**, *112*, 3183.
- (33) Garreau, S.; Louarn, G.; Buisson, J. P.; Froyer, G.; Lefrant, S. *Macromolecules* **1999**, *32*, 6807.
- (34) Sakmeche, N.; Aeiyyach, S.; Aaron, J. J.; Jouini, M.; Lacroix, J. C.; Lacaze, P. C. *Langmuir* **1999**, *15*, 2566.
- (35) Li, C.; Imae, T. *Macromolecules* **2004**, *37*, 2411.
- (36) Greczynski, G.; Kugler, T.; Keil, M.; Osikowicz, W.; Fahlman, M.; Salaneck, W. R. *J. Electron Spectrosc. Relat. Phenom.* **2001**, *121*, 1.
- (37) Randriamahazaka, H.; Plesse, C.; Teysie, D.; Chevrot, C. *Electrochim. Commun.* **2004**, *6*, 299.
- (38) Hsu, C. F.; Zhang, L.; Peng, H.; Sejdic, J. T.; Killmartin, P. A. *Curr. Appl. Phys.* **2008**, *8*, 316.
- (39) Bandaru, P. R. *Applied Science*; Apsara Innovations Pvt. Ltd.: Bangalore, India; 2009; Chapter 5, pp 114–120.
- (40) Yan, K. Y.; Xue, Q. Z.; Zheng, Q. B.; Hao, L. Z. *Nanotechnology* **2007**, *18*, 255705.
- (41) Mustonen, T.; Kordas, K.; Saukko, S.; Toth, G.; Penttila, J. S.; Helisto, P.; Seppa, H.; Jantunen, H. *Phys. Status Solidi* **2007**, *244*, 4336.
- (42) Ren, A.; Pickup, P. G. *J. Phys. Chem.* **1993**, *97*, 5356.
- (43) Ren, X.; Pickup, P. G. *J. Chem. Soc., Faraday Trans.* **1993**, *89*, 321.
- (44) Pickup, P. G. *J. Chem. Soc., Faraday Trans.* **1990**, *86*, 3631.
- (45) Kumar, A.; Welsh, D. M.; Morvant, M. C.; Piroux, F.; Abboud, K. A.; Reynolds, J. R. *Chem. Mater.* **1998**, *10*, 896.
- (46) Granqvist, C. G. *Handbook of Inorganic Electrochromic Materials*; Elsevier Science B.V.: Amsterdam, The Netherlands, 1995.
- (47) Hillman, A. R.; Bruckensrein, S. *J. Chem. Soc., Faraday Trans.* **1993**, *89*, 339.
- (48) Gaupp, C. L.; Welsh, D. M.; Rauh, R. D.; Reynolds, J. R. *Chem. Mater.* **2002**, *14*, 3964.
- (49) Reeves, B. D.; Unur, E.; Ananthkrishnan, N.; Reynolds, J. R. *Macromolecules* **2007**, *40*, 5344.
- (50) Sonnenz, G.; Meng, H.; Wudl, F. *Chem. Mater.* **2004**, *16*, 574–580.
- (51) Schwendeman, I.; Gaupp, C. L.; Hancock, J. M.; Groenendaal, L.; Reynolds, J. R. *Adv. Funct. Mater.* **2003**, *13*, 541.
- (52) Ahonen, H. J.; Lukkari, J.; Kankare, J. *Macromolecules* **2000**, *33*, 6787.

JP9012976